Progress In Electromagnetics Research B, Vol. 46, 79–100, 2013

SOLUTION OF THE ELECTROMAGNETIC SCATTERING PROBLEM FROM AN ELECTRICALLY LARGE RANDOM DIELECTRIC MEDIUM

Bruno Stupfel* and Mikael Picard

CEA, DAM, CESTA, F-33114 Le Barp, France

Abstract—The time-harmonic electromagnetic scattering problem from a random inhomogeneous dielectric medium (here a turbulent plasma wake created by the atmospheric reentry of a vehicle) is considered. The electronic density of the plasma, that gives rise to its dielectric permittivity, has a fluctuating part $\epsilon_f(\underline{r})$, the variance and correlation function of which are known a priori. Because the electrical dimensions of the wake can be very large, the numerical solution of Maxwell's equations via a full-wave calculation performed with a boundary element and finite element method is prohibitive when statistical quantities such as the mean Radar Cross Section (RCS) and its variance are required, that necessitate a large number of random realizations. To remedy this difficulty, two approximations are considered and illustrated for a 2D scattering problem. First, a Mie series approach is adopted where the medium is discretized with small disks, thus reducing considerably the number of unknowns for a given random realization of $\epsilon_f(\underline{r})$, and a domain decomposition method is proposed to further reduce the complexity of the numerical solution of the corresponding system. Second, the statistical mean and the variance of the RCS are derived in closed-form from the Born approximation and yield accurate results when, as expected, the statistical mean of the relative dielectric permittivity is close to unity and $|\epsilon_f(\underline{r})|$ is small. Conversely, it is shown how these expressions can be used to validate the results obtained with the Mie series approximation. Numerical examples are presented that illustrate the potentialities of these techniques.

Received 8 October 2012, Accepted 21 November 2012, Scheduled 24 November 2012

* Corresponding author: Bruno Stupfel (bruno.stupfel@cea.fr).

1. INTRODUCTION

We consider the solution of the time-harmonic electromagnetic scattering problem from a random inhomogeneous dielectric medium such as snow, ice or vegetation canopy where the relative dielectric permittivity $\epsilon(\underline{r})$ has a randomly fluctuating part $\epsilon_f(\underline{r})$. Such is also the case for a turbulent plasma wake created by the atmospheric reentry of a vehicle. The (low) electronic density of the plasma, that gives rise to its dielectric permittivity, has a fluctuating part, the variance and correlation function of which can be estimated a priori. Because the electrical dimensions of the wake can be very large (typically a cone several thousands of wavelengths long with a base several wavelengths large), the numerical solution of Maxwell's equations constitutes a formidable problem, especially when statistical quantities such as the mean Radar Cross Section (RCS) and its variance are required, that necessitate a large number (at least several hundreds) of random realizations. To remedy this difficulty, calculations can be performed for a relatively low cost from various approximations [1]. The Born approximation (BA) is the most straightforward [11] if the statistical means $\epsilon_m(\underline{r}) = \langle\epsilon(\underline{r})\rangle$ of the relative dielectric permittivity are close to unity and $|\epsilon_f(\underline{r})|$ is small: then the mean of the co-polarized RCS is directly obtained from the first term in the Born series via the Fourier transform (FT) of the covariance function [11]. When the cross-polarized RCS is desired, or $|\epsilon_m(\underline{r})-1| \ll 1$ is not satisfied, these quantities can be obtained from the second term in the series but at the cost of a much more elaborate technique that necessitates the calculation of the field and of the Green's function inside the mean medium [12]. However, the convergence of the Born series is not guaranteed and, if it converges, more than two terms may be needed in the series to achieve a reasonable accuracy [13, 14]. For a given random realization of $\epsilon_f(\underline{r})$, the cost of an "exact" numerical solution of this very large problem via a full-wave calculation performed in the frequency domain with a boundary element and finite element method (BE-FEM) is prohibitive even when efficient domain decomposition methods are employed (e.g., [5, 6]). Note that an acceptable accuracy might still be achieved for a smaller cost if the integral equation is replaced by an approximate absorbing boundary condition (ABC-FEM: e.g., [7, 8]). Another possibility is to use a time-domain method such as the PML-FDTD (e.g., [9]), but the very large computational domain implies a very dense mesh and, hence, a very large number of unknowns to minimize the dispersion error. An additional difficulty arises for the FDTD when $\epsilon_f(\underline{r})$ is frequency dependent, as is the case for the plasma originating from an atmospheric reentry, because a random realization of $\epsilon_f(\underline{r})$ must be performed in the whole frequency range of interest and accurately approximated by a simple enough frequency model (e.g., Debye or Lorentz [10]). We have adopted here a Mie series approach in the frequency domain: the medium is discretized with small spheres [16], thus reducing considerably the number of unknowns compared with the BE-FEM. On account of the still very large size of the corresponding linear system and of the ill-conditioned character of its matrix [16], we propose a domain decomposition method (DDM) that reduces the numerical complexity.

As a first approach, we consider here a 2D problem where the dielectric permittivity is invariant along the z axis and fills a rectangle in the (xOy) plane that may be viewed as a cross section of the wake. The organization of this paper is as follows. Section 2 presents the scattering problem and the Mie series solution when the medium is discretized by small disks [15]. In Section 3 we consider the iterative solution of the corresponding linear system, its relationship with the BA, and some DDM solutions. The technique employed for the random realizations of $\epsilon(\underline{r})$ is presented in Section 4. In Section 5 we show how the mean value and the variance of the RCS derived in closed-form from the first term in the BA can be used to check the accuracy of numerical results and, in particular, the correct discretization of the correlation function. Numerical results are presented in Section 6 that illustrate the pertinence of these methods. Conclusions are proposed in Section 7.

2. STATEMENT OF THE PROBLEM AND MIE SERIES SOLUTION

2.1. Statement of the Problem

Without loss of generality, the collision losses are neglected, and a low density plasma is considered: $0 < \epsilon_m(\underline{r}) \leq 1$. The relative dielectric permittivity of the plasma writes $\epsilon(\underline{r}) = 1 - \omega_p^2(\underline{r})/\omega^2$ with $\omega_p^2(\underline{r}) = e^2 N_{el}(\underline{r})/(\epsilon_0 m_e)$. e is the electronic charge, m_e the electronic mass and ϵ_0 is the free space dielectric permittivity. The electronic density has a fluctating part $N_f(\underline{r})$, $N_{el}(\underline{r})(\underline{r}) = \langle N_{el}(\underline{r})\rangle + N_f(\underline{r})$, so that

$$\epsilon_m(\underline{r}) = 1 - C'\langle N_{el}(\underline{r})\rangle, \quad \epsilon_f(\underline{r}) = -C' N_f(\underline{r}) \tag{1}$$

$C' = 80.6/f^2$ where $f = \omega/2\pi$ is the frequency of the incident wave. $\epsilon_f(\underline{r})$ is a random variable (r.v.) with zero mean value and a gaussian probability density function (pdf)

$$p(\epsilon_f, \underline{r}) = \frac{1}{\sqrt{2\pi}\sigma(\underline{r})} \exp\left(- \frac{\epsilon_f^2}{2\sigma^2(\underline{r})} \right) \tag{2}$$

The variance $\sigma^2(\underline{r})$ depends on $\langle N_{el}(\underline{r})\rangle$: $\sigma^2(\underline{r}) = \langle \epsilon_f^2(\underline{r})\rangle = C'^2 \langle N_f^2(\underline{r})\rangle = C'^2 \sigma_N^2(\underline{r})$, and $\sigma_N(\underline{r}) \simeq 0.4\langle N_{el}(\underline{r})\rangle$ [1]. Hence:

$$\begin{aligned} \sigma(\underline{r}) &\simeq 0.4C'\langle N_{el}(\underline{r})\rangle = 0.4\delta\epsilon_m(\underline{r}) \\ \delta\epsilon_m(\underline{r}) &= (1 - \epsilon_m(\underline{r})) \geq 0 \end{aligned} \tag{3}$$

The correlation function of $\epsilon_f(\underline{r})$ is isotropic and approximated by an exponential [1] with correlation length L_c:

$$C_f(r) = \langle \epsilon_f\left(\underline{r}'\right) \epsilon_f\left(\underline{r}' - \underline{r}\right)\rangle = \sigma^2 e^{-r/L_c} \tag{4}$$

(3) and (2) imply

$$\lim_{\epsilon_m(\underline{r})\to 1} \epsilon_f(\underline{r}) = 0 \tag{5}$$

For the atmospheric reentry of a hypersonic vehicle with maximum diameter $D_{\max}$, $\langle N_{el}(\underline{r})\rangle$ is generally comprised between $10^{14}\,\mathrm{m}^{-3}$ and $10^{15}\,\mathrm{m}^{-3}$, and $0.2D_{\max} \leq L_c \leq 0.6D_{\max}$ [2,3]. The wake is typically a cone with length and maximum diameter approximately equal to $100D_{\max}$ and several $D_{\max}$ [4], respectively.

The computational domain V_s is a rectangle in the (xOy) plane, with side lengths L_x, L_y, filled with the random medium. In TM (TE) polarization, the electric (respectively magnetic) field is parallel to the z axis and $u = E_z$ (respectively $u = \eta_0 H_z$ where η_0 is the free space impedance); the time dependence is $e^{i\omega t}$. V_s is illuminated by the plane wave $u^{inc}(r, \varphi) = e^{ik_0 r\cos(\varphi-\varphi_0)}$ where k_0 designates the free space wave number, $(r,\, \varphi)$ the polar coordinates and φ_0 the angle of incidence with respect to the x axis.

2.2. Mie Series Solution

V_s is divided into $N_s = N_x N_y$ square identical small cells where $\epsilon(\underline{r})$ is assumed to be constant. $\Delta_f = L_x/N_x = L_y/N_y$ is the side of the cell so that $N_s = V_s/\Delta_f^2$. Following [15], each cell is replaced by a disk, embedded in free space, with radius $R_f = \Delta_f/\sqrt{\pi}$ so that its surface is equal to Δ_f^2. If (r_j, φ_j) designates the coordinates in the local frame of disk j, the scattered field outside this disk writes $u^s(r_j, \varphi_j) = \sum_{n=-N_{mie}}^{N_{mie}} c_{jn} H_n^{(2)}(k_0 r_j) e^{in\varphi_j}$ while the total field inside the disk is $u^{int}(r_j, \varphi_j) = \sum_{n=-N_{mie}}^{N_{mie}} b_{jn} J_n(k_j r_j) e^{in\varphi_j}$. $H_n^{(2)}(\cdot)$ is the Hankel function of second kind and order n, $J_n(\cdot)$ is the Bessel function of order n and $N_{mie} = E(k_0 R_f) + 1$. $k_j = k_0\sqrt{\epsilon_j}$ where ϵ_j is the value of ϵ in disk j. By enforcing the continuity of the tangential components of the electric and magnetic fields on the circular boundary of disk j, coefficients c_j are solutions of the following $(T \times T)$ system, with $T = N_s(2N_{mie} + 1)$:

$$\mathbf{S}\underline{c} = \underline{a} \tag{6}$$

$$\mathbf{S} = \begin{pmatrix} (S_{11}^{\ln}) & \dots & (S_{1g}^{\ln}) & \dots & (S_{1N_s}^{\ln}) \\ \vdots & \ddots & \vdots & \ddots & \vdots \\ (S_{j1}^{\ln}) & \dots & (S_{jg}^{\ln}) & \dots & (S_{jN_s}^{\ln}) \\ \vdots & \ddots & \vdots & \ddots & \vdots \\ (S_{N_s1}^{\ln}) & \dots & (S_{N_sg}^{\ln}) & \dots & (S_{N_sN_s}^{\ln}) \end{pmatrix} \tag{7}$$

$$\underline{c} = \begin{pmatrix} (c_1^l) \\ \vdots \\ (c_j^l) \\ \vdots \\ (c_{N_s}^l) \end{pmatrix}; \quad \underline{a} = \begin{pmatrix} (a_1^l) \\ \vdots \\ (a_j^l) \\ \vdots \\ (a_{N_s}^l) \end{pmatrix}; \quad -N_{mie} \leq l,\ n \leq N_{mie}$$

where

$$a_j^l = e^{ik_0 r_j \cos(\varphi_j - \varphi_0)} i^l e^{-il\varphi_0} \tag{8}$$

and

$$\begin{aligned} [S_{jg}^{\ln}] &= [b_{jg}^{\ln}], \quad j \neq g \\ &= [d_j^l \delta_{ln}], \quad j = g \end{aligned} \tag{9}$$

$$b_{jg}^{\ln} = H_{l-n}^{(2)}(k_0 d_{jg}) e^{-i(l-n)\varphi_{jg}} \tag{10}$$

(d_{jg}, φ_{jg} designate the distance and the angle between the centers of disks j and g) and, in TM,

$$d_j^l = \frac{\eta_j H_l^{(2)'}(k_0 a_j) J_l(k_j a_j) - H_l^{(2)}(k_0 a_j) J_l'(k_j a_j)}{J_l(k_0 a_j) J_l'(k_j a_j) - \eta_j J_l'(k_0 a_j) J_l(k_j a_j)} \tag{11}$$

where $\eta_j = 1/\sqrt{\epsilon_j}$. d_j^l is obtained in TE from (11) by substituting $1/\eta_j$ to η_j. The far-field is

$$u^s(r, \varphi) = \sqrt{\frac{2i}{\pi k_0 r}} e^{-ik_0 r} F(\varphi) \tag{12}$$

where

$$F(\varphi) = \sum_{g=1}^{N_s} e^{ik_0 r_g \cos(\varphi_g - \varphi)} \sum_{n=-\infty}^{\infty} c_{gn} i^n e^{in\varphi} \tag{13}$$

and the bistatic RCS is:

$$s(\varphi) = \frac{4}{k_0} |F(\varphi)|^2 \tag{14}$$

This method is termed MIE in what follows. The results obtained with MIE have been compared to those obtained from a 2D BE-FEM code [21], and a reasonable accuracy has been achieved for $0.1 \leq \epsilon \leq 1^\dagger$. As an example, Fig. 1 plots the monostatic RCS obtained on a square of side 60 cm for $f = 1$ GHz. The four quadrants of the square are filled with four different homogeneous dielectrics. The BE-FEM results are obtained with $N_{\mathrm{FE}} = 67500$ volume unknowns and $N_S = 600$ surface unknowns. This implies that the sparse FE system must be solved N_S times, and a full complex ($N_S \times N_S$) system, that corresponds to the integral equation prescribed on the boundary of V_S, must be solved once. As a comparison, MIE involves the solution of a full, complex, (432×432) system. We observe on Fig. 1 that MIE yields less acurate results in TE when the wave is incident on the edges of the square ($\varphi = 45°$, $135°$, $225°$, $315°$). This is probably due to the fact that the edge diffraction is not correctly accounted for by the rounded edges made up by the disks. Actually, this is of no great concern because the cross-section of a wake has no edges (the electronic density goes to zero on its boundary).

3. SOLUTION OF THE MIE SYSTEM

The condition number of matrix **S** as defined in (7) increases rapidly with T [16]. This implies that the iterative solution of (6) via a Krylov technique is efficient only if some preconditioner is employed. However, the cartesian mesh of V_s entails that **S** is almost block-Toeplitz. As a consequence, its computation and storage are $O(T)$ and the cost of a matrix-vector product is $O(T \log N_s)$ [16]. In Section 3.1 we consider a Jacobi iterative solution of (6), and mention its connection with the BA. A DDM approach is presented in Section 3.2.

† For smaller values of ϵ, we have observed that accurate results in TE are obtained only with very dense meshes (for the BE-FM), or a very large number of disks for MIE.

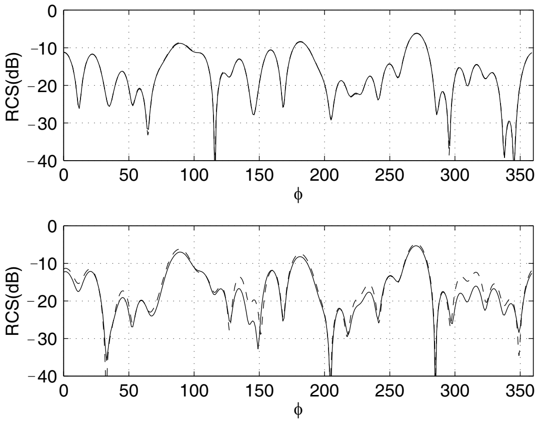

Figure 1. Monostatic RCS versus φ. $f = 1\,\mathrm{GHz}$, N_s=144 ($T = 432$), $L_x = L_y = 60\,\mathrm{cm}$. 4 materials: $\epsilon_1 = 0.7$, $\epsilon_2 = 0.5$, $\epsilon_3 = 0.6$, $\epsilon_4 = 0.8$. Solid line: BE-FEM; dashed line: MIE. Top: TM; bottom: TE.

3.1. Jacobi Solution of (6). Connection with the BA

Let $\mathbf{S} = \mathbf{M} - \mathbf{N}$. Then

$$\underline{c} = \mathbf{M}^{-1}\underline{a} + \sum_{\ell=1}^{\infty} \left(\mathbf{M}^{-1}\mathbf{N}\right)^{\ell} \mathbf{M}^{-1}\underline{a} \tag{15}$$

This series converges only if $\rho(\mathbf{M}^{-1}\mathbf{N}) < 1$ where ρ designates the spectral radius of the matrix. In the Jacobi solution, $\mathbf{M}$ is the diagonal of $\mathbf{S}$ and (15) is then the Neumann series. The first term in (15) does not take into account multiple interactions between the disks. It is shown in Appendix A.1 that

$$\forall \underline{r} \in V_s \quad \delta\epsilon_m(\underline{r}) \ll 1 \Longrightarrow \rho \ll 1 \tag{16}$$

Then (15) reduces to a few matrix-vector products. Also, if the following conditions are satisfied

$$k_0 a_i \ll 1 \ \forall i \tag{17}$$

it is shown in Appendix A.2.2 that the RCS computed from $\mathbf{M}^{-1}\underline{a}$ is equal to the one obtained from the first term in the BA for which the scattered far-field, defined by (12), writes, up to the first order in ϵ_f and $\delta\epsilon_m$ (see Appendix A.2.1):

$$\underline{F}_{\mathrm{BA}}(\varphi) = -i\frac{k_0^2}{4}\underline{W}(\varphi)[F_f(\varphi) - F_m(\varphi)]$$

$$
\begin{aligned}
&F_f(\varphi) = \int_{V_s} \epsilon_f \left(\underline{r}'\right) e^{i\underline{v}\cdot\underline{r}'} d\underline{r}'; \quad F_m(\varphi) = \int_{V_s} \delta\epsilon_m \left(\underline{r}'\right) e^{i\underline{v}\cdot\underline{r}'} d\underline{r}' \\
&\underline{v} = k_0 \left(\widehat{\underline{r}} - \widehat{\underline{k}}\right); \quad \widehat{\underline{k}} = -(\cos\varphi_0, \sin\varphi_0)^t; \quad \widehat{\underline{r}} = (\cos\varphi, \sin\varphi)^t \\
&\text{TM}: \ \underline{W}(\varphi) = \widehat{\underline{z}}; \quad \text{TE}: \ \underline{W}(\varphi) = \underline{V} - \widehat{\underline{r}}\left(\widehat{\underline{r}}\cdot\underline{V}\right) \\
&\underline{V} = (-\sin\varphi_0, \cos\varphi_0)^t
\end{aligned} \tag{18}
$$

$\widehat{\underline{k}}$ and $\widehat{\underline{r}}$ designate the directions of incidence and observation and $\widehat{\underline{z}}$ is the unitary vector along z (superscript t is for transpose). F_m is the far-field scattered by the mean medium $\epsilon_m(\underline{r})$ and F_f is the fluctuating far-field.

3.2. DDM Solution

The non diagonal terms in $\mathbf{S}$ are the coefficients $b_{jg}^{\ln}$ defined in (10) that decrease like $1/\sqrt{d_{jg}}$ when the distance d_{jg} between disks j and g is large. If V_s is partitioned into subdomains Ω_i, we may take advantage of the fact that the matrix elements corresponding to the interaction between distant subdomains are small. For example, if V_s is a rectangle partitioned into three subdomains along its largest dimension, with Ω_2 located in between Ω_1 and Ω_3, (6) writes:

$$
\begin{pmatrix} \mathbf{S}_{11} & \mathbf{S}_{12} & \mathbf{S}_{13} \\ \mathbf{S}_{21} & \mathbf{S}_{22} & \mathbf{S}_{23} \\ \mathbf{S}_{31} & \mathbf{S}_{32} & \mathbf{S}_{33} \end{pmatrix} \begin{pmatrix} \underline{c}_1 \\ \underline{c}_2 \\ \underline{c}_3 \end{pmatrix} = \begin{pmatrix} \underline{a}_1 \\ \underline{a}_2 \\ \underline{a}_3 \end{pmatrix} \tag{19}
$$

We let $\mathbf{S} = \mathbf{M} - \mathbf{N}$ with

$$
\text{DDM1}: \quad \mathbf{M} = \begin{pmatrix} \mathbf{S}_{11} & \mathbf{S}_{12} & 0 \\ \mathbf{S}_{21} & \mathbf{S}_{22} & \mathbf{S}_{23} \\ 0 & \mathbf{S}_{32} & \mathbf{S}_{33} \end{pmatrix} \tag{20}
$$

and (6) is solved via (15). Because $\rho(\mathbf{M}^{-1}\mathbf{N}) = 0$ if $\mathbf{S}_{13} = \mathbf{S}_{31} = 0$ we may expect that (15) converges rapidly if $||\mathbf{S}_{13}||, ||\mathbf{S}_{31}|| \ll 1$, i.e., if the distance between Ω_1 and Ω_3 is large enough. But $\mathbf{M}\underline{c} = \underline{a}$ must be solved for each iteration. Alternatively, if

$$
\text{DDM2}: \quad \mathbf{M} = \begin{pmatrix} \mathbf{S}_{11} & 0 & 0 \\ 0 & \mathbf{S}_{22} & 0 \\ 0 & 0 & \mathbf{S}_{33} \end{pmatrix} \tag{21}
$$

then $\mathbf{M}$ is block diagonal and, provided that $\rho(\mathbf{M}^{-1}\mathbf{N}) < 1$, three independent systems $\mathbf{M}_i\underline{c}_i = \underline{a}_i$ ($\mathbf{M}_i = \mathbf{S}_{ii}$) are to be solved in Ω_i, that may be done via a Jacobi, as in Section 5.1, if $\rho_i = \rho(\mathbf{M}_i^{-1}\mathbf{N}_i) < 1$, $1 \le i \le 3$.

4. RANDOM REALIZATIONS OF $\epsilon(\underline{r})$

Let V_t be a rectangle $(L_{tx} \times L_{ty})$ with $L_{tx} = L_x + 2\Delta L_t$, $L_{ty} = L_y + 2\Delta L_t$ (V_s is in the middle of V_t). V_t is partitioned into N_t cells $(\Delta_f \times \Delta_f)$. First, N_t random independent realizations (white gaussian noise) are performed in V_t, the pdf of which is given by (2) with $\sigma(\underline{r}) = \sigma$ as defined in (3). The N_t values of $\epsilon(\underline{r}) = \epsilon_g(\underline{r})$ are attributed to each of the N_t cells. If $\hat{\epsilon}_g$ designates the discrete FT (DFT) of ϵ_g in V_t, we get:

$$\left\langle |\hat{\epsilon}_g(\underline{k})|^2 \right\rangle = \left\langle \epsilon_g^2 \right\rangle V_t^2 / N_t = \sigma^2 V_t^2 / N_t \tag{22}$$

Let $\Phi_f(k)$ be the FT of the correlation function $C_f(r)$:

$$\Phi_f(k) = \int_{\mathcal{R}^2} C_f(r) e^{-2i\pi \underline{k}.\underline{r}} d\underline{r} = \frac{2\pi\sigma^2 L_c^2}{[1 + (2\pi k L_c)^2]^{3/2}} \tag{23}$$

Then $\hat{\epsilon}_g(\underline{k})$ is multiplied by $\Phi_f(k)$ to obtain the FT of $\epsilon_f(\underline{r})$:

$$\hat{\epsilon}_f(\underline{k}) = \hat{\epsilon}_g(\underline{k}) \sqrt{\frac{N_t \Phi_f(k)}{\sigma^2 V_t}} \tag{24}$$

(24) and (22) imply $\langle |\hat{\epsilon}_f(\underline{k})|^2 \rangle = V_t \Phi_f(k)$ thus ensuring that $C_f(r)$ is the correlation function of $\epsilon_f(\underline{r})$. The inverse FT of $\hat{\epsilon}_f(\underline{k})$ yields $\epsilon_f(\underline{r})$:

$$\begin{aligned} \epsilon_f(\underline{r}) &= \sqrt{\frac{N_t}{V_t}} \int_{V_t} \epsilon_g\left(\underline{r}'\right) \Psi_f\left(\left|\underline{r} - \underline{r}'\right|\right) d\underline{r}' \\ \Psi_f(r) &= \int_{\mathcal{R}^2} \tilde{\Phi}_f(k) e^{2i\pi \underline{k}.\underline{r}} d\underline{k}; \quad \tilde{\Phi}_f(k) = \sqrt{\Phi_f(k)/\sigma^2} \end{aligned} \tag{25}$$

We easily get [19]:

$$\begin{aligned} &\Psi_f(r) = \frac{1}{L_c} \tilde{\Psi}_f(r/L_c); \quad \tilde{\Psi}_f(x) = \frac{\sqrt{\pi} e^{5i\pi/8}}{2^{5/4} \Gamma(3/4) x^{1/4}} H_{1/4}^{(1)}(ix) \in \mathbb{R}^+ \\ &x \to 0: \ \tilde{\Psi}_f(x) \sim \tilde{\Psi}_f^{\text{sing}}(x) = \frac{\sqrt{\pi}}{2\sin(\pi/4)\Gamma^2(3/4)\sqrt{x}} \end{aligned} \tag{26}$$

where $H_{1/4}^{(1)}(\cdot)$ is the Hankel function of the first kind and order 1/4 and $\Gamma(\cdot)$ is the gamma function. When $x \to \infty$, $\tilde{\Psi}_f(x)$ behaves like e^{-x}. Then we may replace, in the integral over V_t involved in the definition (25) of $\epsilon_f(\underline{r})$, V_t by the disk B_r of center $\underline{r}$ and radius $R_t = \beta L_c$: $B_r = \{\underline{r}' \setminus |\underline{r} - \underline{r}'| \leq R_t\}$ and

$$\epsilon_f(\underline{r}) \simeq \sqrt{\frac{N_t}{V_t}} \int_{B_r} \epsilon_g\left(\underline{r}'\right) \Psi_f\left(\left|\underline{r} - \underline{r}'\right|\right) d\underline{r}' \tag{27}$$

If

$$\Delta_f = L_c/\alpha_f \tag{28}$$

then

$$\begin{aligned} &\Delta L_t = R_t = \alpha_f \beta \Delta_f \\ &N_t = L_{tx} L_{ty}/\Delta_f^2; \quad N_s = L_x L_y/\Delta_f^2 \end{aligned} \tag{29}$$

For a given cell i in V_s ($1 \leq i \leq N_s$), $\underline{r}_i$ designates the center of the cell and $\epsilon_f(\underline{r}_i)$ in (27) is evaluated as follows:

$$\begin{aligned} \epsilon_f(\underline{r}_i) &= \sqrt{\frac{N_t}{V_t L_c}} \sum_{j=1}^{N_v} I_{ij} \epsilon_{gj} \\ I_{ij} &= \int_{V_j} \tilde{\Psi}_f \left(\left| \underline{r}_i - \underline{r}' \right| / L_c \right) d\underline{r}' \end{aligned} \tag{30}$$

N_v (independent of i) is the number of disks in B_{r_i} and ϵ_{gj} is the value of $\epsilon_g(\underline{r}')$ in one of these disks V_j with surface Δ_f^2. When $i = j$, we write $\tilde{\Psi}_f(x) = \tilde{\Psi}_f^{\text{sing}}(x) + (\tilde{\Psi}_f(x) - \tilde{\Psi}_f^{\text{sing}}(x))$, integrate exactly $\tilde{\Psi}_f^{\text{sing}}(x)$ and use a four point quadrature formula for the disk [20] (that serves also to compute I_{ij} for $i \neq j$) to integrate the non singular function $\tilde{\Psi}_f(x) - \tilde{\Psi}_f^{\text{sing}}(x)$. The values of $\tilde{\Psi}_f(x)$ are calculated once and tabulated. When N_s is large, and on account of the symmetries, the total number of I_{ij} that need to be calculated is approximately equal to $(\beta L_c)^2 N_s/(8 L_x L_y)$ and the cost of the matrix-vector product in (30) is $O[(\beta L_c N_s)^2/(8 L_x L_y)]$.

If $\hat{\epsilon}_g$ (ϵ_f) is calculated via a DFT from ϵ_g (respectively $\hat{\epsilon}_f$ in (24)) [17, 18] then, because of the DFT aliasing, the size of V_t is much larger (typically $L_{tx}, L_{ty} \geq 100 L_c$) than the one required by the above technique, and the cost $O(N_t \log N_t)$ of the DFT becomes prohibitive for the values of N_s used in this paper. Numerical experiments show that $\alpha_f \geq 5$ and $\beta = 3$ yield an reasonable accuracy (see Fig. 2).

5. STATISTICAL MEAN AND VARIANCE OF THE RCS DERIVED FROM THE FIRST TERM IN THE BA

From (14) and (18), the RCS of the first term in the BA writes $s_{\text{BA}}(\varphi) = k_0^3 \chi(\varphi) |F_f(\varphi) - F_m(\varphi)|^2/4$ with $\chi(\varphi) = ||\underline{W}(\varphi)||^2$ that entails, because $\epsilon_f(\underline{r})$ and $\delta\epsilon_m(\underline{r})$ are real, $s_{\text{BA}}(\varphi) = \frac{k_0^3}{4} \chi(\varphi) \int_{V_s \times V_s} (\epsilon_f(\underline{r}') - \delta\epsilon_m(\underline{r}'))(\epsilon_f(\underline{r}'') - \delta\epsilon_m(\underline{r}'')) e^{i\underline{v}\cdot(\underline{r}' - \underline{r}'')} d\underline{r}' d\underline{r}''$. Hence

$$s_{\text{BA}}(\varphi) = s_f(\varphi) + s_m(\varphi) - 2\text{Re}(s_{mf}(\varphi))$$

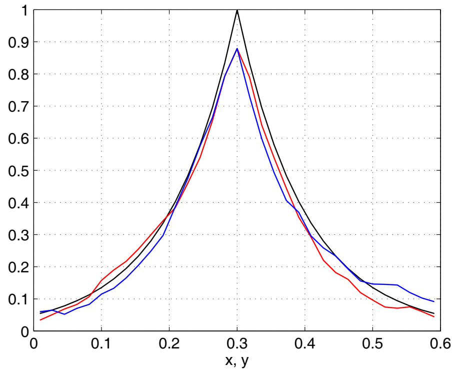

Figure 2. $L_x = L_y = 60\,\mathrm{cm}$, $L_c = 10\,\mathrm{cm}$, $\sigma = 1$, $\alpha_f = 5.5$, $\beta = 3$. $N_s = 33 \times 33$ and $N_t = 67 \times 67$ ($L_{tx} = L_{ty} = 1.22\,\mathrm{m}$). Dark line: exact correlation function $C_f(\underline{r})$ as defined in (4). Red and blue lines: numerical correlation function $C_f^{num}(\underline{r}) = \langle \epsilon_f(\underline{r}')\epsilon_f(\underline{r}' - \underline{r})\rangle$ (the mean is calculated on 1000 random realizations); $\underline{r}' = (0.3, 0.3)$ is the center of V_s and $\underline{r} = (x_j, 0.3)$ (red line: $C_f^{num}(x_j, 0.3)$) or $\underline{r} = (0.3, y_j)$ (blue line: $C_f^{num}(0.3, y_j)$) where (x_j, y_j) are the coordinates of the center of cell j.

$$\begin{aligned} s_m(\varphi) &= \frac{k_0^3}{4}\chi(\varphi)|F_m(\varphi)|^2 \\ s_f(\varphi) &= \frac{k_0^3}{4}\chi(\varphi)|F_f(\varphi)|^2 \\ s_{mf}(\varphi) &= \frac{k_0^3}{4}\chi(\varphi)F_f(\varphi)F_m^*(\varphi) \end{aligned} \tag{31}$$

with

$$\text{TM: } \chi(\varphi) = 1; \quad \text{TE: } \chi(\varphi) = \cos^2(\varphi - \varphi_0) \tag{32}$$

s_m is the RCS of the mean medium $\epsilon_m(\underline{r})$. Note that, because $\delta\epsilon_m(\underline{r}) \geq 0$, $|F_m(\varphi)|^2 \leq \int_{V_s} \delta\epsilon_m^2(\underline{r}) = |F_m(\pi + \varphi_0)|^2$. Since $\chi(\pi + \varphi_0) = 1$, we get

$$\max_{\varphi} s_m(\varphi) = s_m(\pi + \varphi_0) = \frac{k_0^3}{4}\left[\int_{V_s} \delta\epsilon_m(\underline{r})d\underline{r}\right]^2 \tag{33}$$

We know derive the statistical mean $\langle s_{\mathrm{BA}}(\varphi)\rangle$. Because $\langle \epsilon_f(\underline{r})\rangle = 0$, $\langle s_{mf}(\varphi)\rangle = 0$ and

$$\langle s_{\mathrm{BA}}(\varphi)\rangle = \langle s_f(\varphi)\rangle + s_m(\varphi) \tag{34}$$

$\langle s_f(\varphi)\rangle$ is proportional to $\langle|F_f(\varphi)|^2\rangle = \int_{V_s\times V_s}\langle\epsilon_f(\underline{r}')\epsilon_f(\underline{r}'')\rangle e^{i\underline{v}\cdot(\underline{r}'-\underline{r}'')}d\underline{r}'d\underline{r}''$ that writes, because $\langle\epsilon_f(\underline{r}')\epsilon_f(\underline{r}'')\rangle = C_f(\underline{r}'-\underline{r}'')$,

$$\begin{aligned}\langle|F_f(\varphi)|^2\rangle &= \int_{V_s\times V_s} C_f(r)e^{i\underline{v}\cdot\underline{r}}d\underline{r}d\underline{r}'' = V_s\int_{V_s} C_f(r)e^{i\underline{v}\cdot\underline{r}}d\underline{r} \\ &\simeq V_s\int_{\mathbb{R}^2} C_f(r)e^{i\underline{v}\cdot\underline{r}}d\underline{r} = V_s\Phi_f(v/2\pi)\end{aligned} \tag{35}$$

The last identity in (35), where V_s is replaced by $\mathbb{R}^2$, is justified if $C_f(L/2) \ll C_f(0)$, with $L = \min(L_x, L_y)$, because $C_f(r)$ decreases exponentially with r. As a consequence:

$$\begin{aligned}&C_f(L/2)/C_f(0) \ll 1 \Longrightarrow \\ &\langle s_f(\varphi)\rangle \simeq \frac{k_0^3V_s}{4}\chi(\varphi)\Phi_f(v/2\pi) \simeq \frac{k_0^3V_s}{4}\chi(\varphi)\Phi_f\left(\frac{k_0}{\pi}\left|\cos\frac{\varphi-\varphi_0}{2}\right|\right)\end{aligned} \tag{36}$$

when $L\to\infty$, it is shown in Appendix A.3 that the variance $\Sigma^2_{\mathrm{BA}}(\varphi) = \langle s_{\mathrm{BA}}(\varphi)^2\rangle - \langle s_{\mathrm{BA}}(\varphi)\rangle^2$ of the RCS is given by:

$$\begin{aligned}&\Sigma^2_{\mathrm{BA}}(\varphi) = \Sigma^2_f(\varphi) + \Sigma_{mf}(\varphi); \quad \Sigma_f(\varphi) \simeq \sqrt{2}\langle s_f(\varphi)\rangle \\ &\Sigma_{mf}(\varphi) \simeq \frac{k_0^6}{8}\chi^2(\varphi)\Phi_f(v/2\pi)\left\{V_s\left|F_m(\underline{v})\right|^2 + \mathrm{Re}\left[F_m^2(\underline{v})J_V(\underline{v})\right]\right\}\end{aligned} \tag{37}$$

$J_V(\underline{v})$ is defined by (A9) in Appendix A.3.

6. NUMERICAL RESULTS

We present in Section 6.1 results obtained with the solution of (6) and the BA presented in Sections 3 and 4. DDM performances are investigated in Section 6.2.

6.1. Performances of MIE and the BA for the Computation of the Statistics of the RCS

V_s is a square with side length $L = 60\,\mathrm{cm}$, ϵ_m is constant, $L_c = 10\,\mathrm{cm}$ and σ is defined as in (3). A random realization of $\epsilon_f(\underline{r})$ in V_s is performed with $\beta = 3$ in (29). For the $\varphi_0 = 40°$ incidence, the bistatic RCS, $\mathrm{RCS}_{\mathrm{MIE}}(\varphi) = 10\log(s(\varphi))$, is computed with MIE ($T = 3N_s$). The mean value of the RCS, $\langle\mathrm{RCS}_{\mathrm{MIE}}(\varphi)\rangle = 10\log\langle s(\varphi)\rangle$, and its least square deviation (l.s.d.) Σ_{MIE} are computed on 400 random realizations. The RCS of the mean medium ϵ_m, $\mathrm{RCS}_{\epsilon_m}$, is computed with the BE-FEM code. Regarding the BA, the mean RCS, $\langle\mathrm{RCS}_{\mathrm{BA}}(\varphi)\rangle = 10\log\langle s_{\mathrm{BA}}(\varphi)\rangle$, its l.s.d. $\Sigma_{\mathrm{BA}}(\varphi)$ and the mean fluctuating RCS, $\langle\mathrm{RCS}_f(\varphi)\rangle = 10\log\langle s_f(\varphi)\rangle$, are calculated with

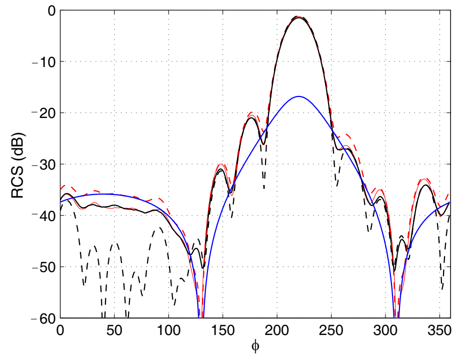

Figure 3. Bistatic RCS. $f = 1\,\text{GHz}$, $\varphi_0 = 40°$, $\epsilon_m = 0.95$, $N_s = 25 \times 25$. $\langle \text{RCS}_{\text{MIE}}^{exact} \rangle$ (black solid line), $\langle \text{RCS}_{\text{MIE}}^{\ell=0} \rangle$ (red solid line), RCS_{ϵ_m} (BE-FEM: black dashed line), $\langle \text{RCS}_{\text{BA}} \rangle$ (red dashed line), $\langle \text{RCS}_f \rangle$ (blue solid line).

formulas (34), (36) and (37). The results, obtained for $\epsilon_m = 0.95$ and $\epsilon_m = 0.7$, are presented in TE polarization only where the accuracy is the poorest (see Fig. 1). We recall that ϵ_m is related to the mean electronic density and the frequency as indicated in (1). $N_s = 25 \times 25$ ($T = 1875$), $\alpha_f = 4.2$ in (28) and $\beta = 3$.

6.1.1. $\epsilon_m = 0.95 \Rightarrow \sigma = 0.02$

For $f = 1\,\text{GHz}$, the RCS computed with Jacobi converges in two iterations, i.e., the three first terms only in (15) are necessary. The FEM has converged for $N_{\text{FE}} = 67500$ and $N_S = 600$. In view of Fig. 3, the following observations can be made:

– The mean RCS $\langle \text{RCS}_{\text{MIE}}^{\ell=0}(\varphi) \rangle$ computed from the first term in (15) is close to the exact one $\langle \text{RCS}_{\text{MIE}}^{exact}(\varphi) \rangle = \langle \text{RCS}_{\text{MIE}}^{\ell=2}(\varphi) \rangle$ [this comes from $\epsilon_m \simeq 1$: see (16)] and

$$\left\langle \text{RCS}_{\text{MIE}}^{\ell=0}(\varphi) \right\rangle \simeq \langle \text{RCS}_{\text{BA}}(\varphi) \rangle \tag{38}$$

On account of the fact that the first term in (15) yields the BA if (17) is satisfied then, provided that $C_f(L/2)/C_f(0) \ll 1$ in (36) is also satisfied (here $C_f(L/2)/C_f(0) = 0.05$), (38) ensures that V_s and the correlation function are correctly discretized. This is important because (38) can be used to check the accuracy of the numerical results obtained with MIE.

– When the RCS of the mean medium is much larger than the mean of its fluctuating part ($s_m(\varphi) \gg \langle s_f(\varphi) \rangle$) then

$$\left\langle \text{RCS}_{\text{MIE}}^{exact}(\varphi) \right\rangle \simeq \text{RCS}_{\epsilon_m}(\varphi) \tag{39}$$

that, once again, validates the MIE results.

– $s_m(\varphi)$ is maximum for $\varphi_0 = \pi + \varphi$, accordingly to (33). Finally, Fig. 4 shows that Σ_{BA} yields a good approximation of Σ.

Similar conclusions hold for $f = 3\,\mathrm{GHz}$ (the RCS computed with Jacobi converges in 5 iterations; see Figs. 5 and 6). Note that the FEM converges for a denser mesh only ($N_{\mathrm{FE}} = 270000$, $N_S = 1200$).

6.1.2. $\epsilon_m = 0.7 \Rightarrow \sigma = 0.12$

The RCS computed for $f = 400\,\mathrm{MHz}$ with Jacobi converges in 5 iterations. In view of Fig. 7, identities (38) and (39) are satisfied that validate the MIE results, and multiple interactions are not negligible for values of φ where $\langle \mathrm{RCS}_{\mathrm{MIE}}^{\ell=0}(\varphi)\rangle \neq \langle \mathrm{RCS}_{\mathrm{MIE}}^{\ell=5}(\varphi)\rangle$ and $\Sigma_{\mathrm{BA}} \neq \Sigma$ (see Fig. 8). Multiple interactions are even more important at 1 GHz

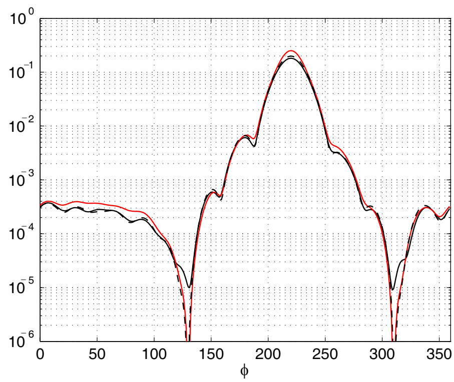

Figure 4. Least square deviation versus φ for the same configuration as in Fig. 3. $\Sigma_{\mathrm{MIE}}^{\ell=0}$ (black dashed line), $\Sigma_{\mathrm{MIE}}^{exact}$ (black solid line), Σ_{BA} (red solid line).

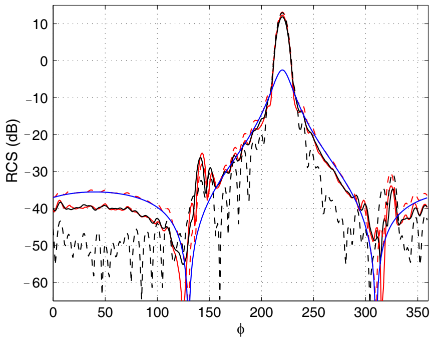

Figure 5. Same captions as in Fig. 3 except for $f = 3\,\mathrm{GHz}$.

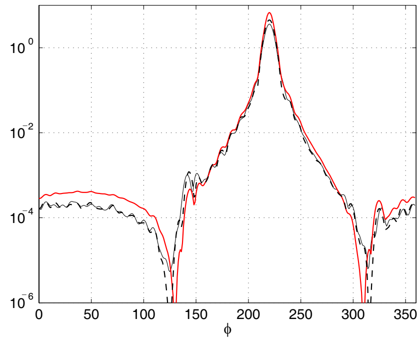

Figure 6. Same captions as in Fig. 4 except for $f = 3\,\mathrm{GHz}$.

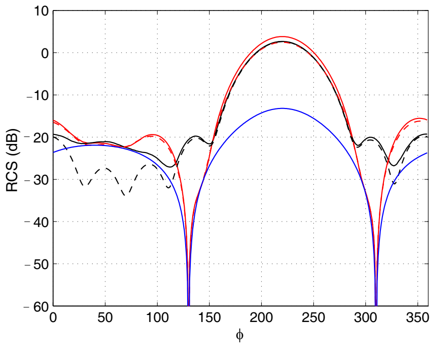

Figure 7. Same captions as in Fig. 3 except for $f = 400\,\text{MHz}$ and $\epsilon_m = 0.7$.

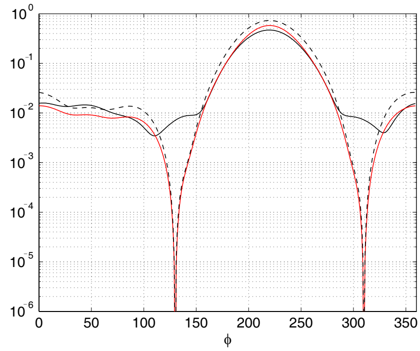

Figure 8. Same captions as in Fig. 4 except for $f = 400\,\text{MHz}$ and $\epsilon_m = 0.7$.

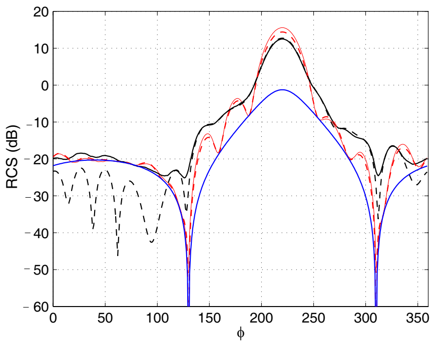

Figure 9. Same captions as in Fig. 3 except for $f = 1\,\text{GHz}$ and $\epsilon_m = 0.7$.

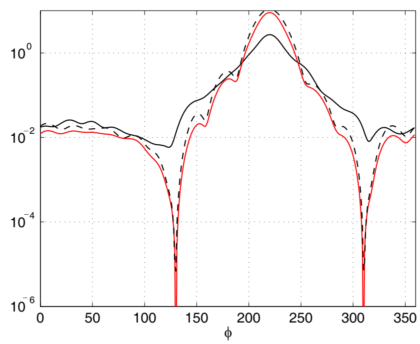

Figure 10. Same captions as in Fig. 4 except for $f = 1\,\text{GHz}$ and $\epsilon_m = 0.7$.

and the Jacobi does not converge (then system (6) is solved directly). Figs. 9 and 10 show that $\langle \text{RCS}^{\ell=0}_{\text{MIE}} \rangle \neq \langle \text{RCS}^{exact}_{\text{MIE}} \rangle$ and $\Sigma_{\text{BA}} \neq \Sigma$ in a larger angular range.

6.2. Performances of the Iterative and DDM Solutions

V_s is now a rectangle with sides $L_x = 60\,\text{cm}$ and $L_y = 20\,\text{cm}$, partitioned into three identical subdomains Ω_i along L_x. $f = 1\,\text{GHz}$, $\epsilon_m = 0.6$, $\sigma = 0.16$, $N_s = 27 \times 9$, $\alpha = 4.5$ and $\beta = 3$. All the calculations are performed with MIE on the random realization of $\epsilon(\underline{r})$ represented in Fig. 11. MIE yields the following values for the spectral radius ρ of matrix $\mathbf{M}^{-1}\mathbf{N}$: $\rho(Jacobi) = 0.86$ [$\mathbf{M} = \text{diag}(\mathbf{S})$], $\rho(GS) = 0.4$ [Gauss-Seidel: $\mathbf{M}$ is the lower triangular part of $\mathbf{S}$], $\rho(\text{DDM1}) = 0.077$ [$\mathbf{M}$ is defined in (20)], $\rho(\text{DDM2}) = 0.35$ [$\mathbf{M}$ is

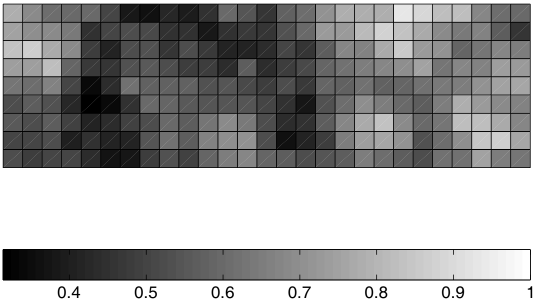

Figure 11. Rectangle $L_x = 60\,\mathrm{cm}$, $L_y = 20\,\mathrm{cm}$: a realization of $\epsilon(\underline{r})$ for $\epsilon_m = 0.6$, $\sigma = 0.16$, $L_c = 10\,\mathrm{cm}$ and $N_s = 27 \times 9$. Color bar: values of $\epsilon(\underline{r})$.

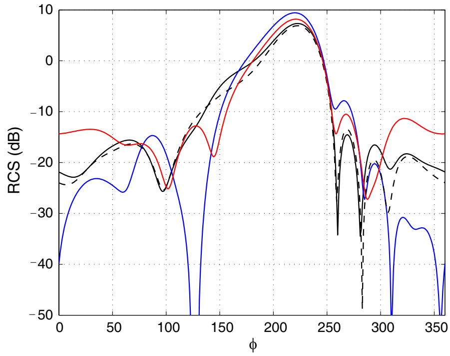

Figure 12. Bistatic RCS obtained with MIE ($T = 729$) for the realization of Fig. 11. $f = 1\,\mathrm{GHz}$ and $\varphi_0 = 40°$. Exact (black solid line), Jacobi $\ell = 0$ (blue solid line), DDM1 $\ell = 0$ (black dashed line), DDM2 $\ell = 0$ (red solid line).

defined in (21)], and these methods converge in, respectively, 28, 8, 2 and 5 iterations. For the DDM2, the spectral radius ρ_1 of $\mathbf{M}_1^{-1}\mathbf{N}_1$ corresponding to the solution of the system in Ω_1 only is $\rho_1 = 0.73$. We observe on Fig. 12 that the RCS obtained with DDM1 and $\ell = 0$ is close to the exact one.

7. CONCLUSIONS

The computation of the RCS by the Mie series has been validated for $0.1 < \epsilon \leq 1$ (see [15] for larger values of ϵ), and the considerable reduction of the numerical complexity with respect to the BE-FEM method has been displayed. The convolution technique proposed for the random realizations of $\epsilon(\underline{r})$ is computationally efficient when the number of cells is not too large. Provided that V_s is large enough, the mean and the variance of the RCS have been derived in closed-form from the BA up to the first order in ϵ_f and $\delta\epsilon_m$, and serve to validate the discretization of V_s used for MIE and of the correlation function. When ϵ_m is close to unity, they yield values close to those obtained from a large number of MIE calculations performed for each random realization, thus leading to a considerable reduction of the computational time. For smaller values of ϵ_m, the Jacobi or Neumann series either do not converge or converge slowly, depending on the importance of the multiple interactions. In this case, it has been shown how DDM1 or DDM2 may be used to accelerate the convergence. DDM1 is computationally more expensive, but the first term in the corresponding series may yield a reasonable accuracy. For DDM2, systems $\mathbf{M}_i\underline{c}_i = \underline{a}_i$ can be solved independently for each subdomain. These techniques can be extended to 3D problems (see, e.g., [16, 22, 23]) to compute, e.g., the statistics of the RCS of the wake created by a hypersonic vehicle during its atmospheric reentry, or else by a satellite in the ionosphere.

APPENDIX A.

A.1. Proof of (16)

From (7) and (9), submatrices S_{jj}^{ln} $(1 \le j \le N_s)$ of $\mathbf{S}$ are diagonal. Let $\mathbf{N} = \mathbf{M} - \mathbf{S}$ with $\mathbf{M} = \mathrm{diag}(\mathbf{S})$. Then submatrices $j = g$ of $\mathbf{N}$ are zero, that implies the same result for $\mathbf{M}^{-1}\mathbf{N}$. Hence, if $\mathbf{X} = -\mathbf{M}^{-1}\mathbf{N}$, the eigenvalues λ of $\mathbf{X}$ are solution of

$$\det(\lambda\mathbf{I} - \mathbf{X}) = \det\begin{pmatrix} \left(\lambda\delta_{\mathrm{ln}}\right) & \dots & \left(X_{1j}^{\mathrm{ln}}\right) & \dots & \left(X_{1M}^{\mathrm{ln}}\right) \\ \vdots & \ddots & \vdots & \ddots & \vdots \\ \left(X_{j1}^{\mathrm{ln}}\right) & \dots & \left(\lambda\delta_{\mathrm{ln}}\right) & \dots & \left(X_{jM}^{\mathrm{ln}}\right) \\ \vdots & \ddots & \vdots & \ddots & \vdots \\ \left(X_{M1}^{\mathrm{ln}}\right) & \dots & \left(X_{Mj}^{\mathrm{ln}}\right) & \dots & \left(\lambda\delta_{\mathrm{ln}}\right) \end{pmatrix}$$

Because $\mathbf{M}^{-1}$ is diagonal, $X_{jg}^{nl} \propto \delta_{jg}/d_j^n$ where d_j^n is defined in (11). In what follows, subindex j of the disk of radius a and permittivity $\epsilon = \epsilon_m + \epsilon_f$ is omitted to alleviate the notations. If $\delta\epsilon_m = 1 - \epsilon_m \ll 1$ then $\epsilon_f' = \epsilon_f + \epsilon_m - 1$ with $|\epsilon_f'| \ll 1$ because of (5), and $k = k_0\sqrt{\epsilon} \sim k_0(1 + \epsilon_f'/2)$. In TM, $\eta = 1/\sqrt{\epsilon}$ that entails, up to the first order in ϵ_f',

$$1/d_j^n \sim i\pi x\epsilon_f' \left\{ J_n(x)J_n'(x) + k_0 a \left[J_n(x)J_n''(x) - J_n'^2(x) \right] \right\} /4 \quad \text{(A1)}$$

$x = k_0 a$ and $J'_n(x)$ and $J''_n(x)$ designate the first and second derivatives of $J_n(x)$ with respect to x. (A1) implies $\lim\limits_{\epsilon'_f \to 0} X^{nl}_{jg} = 0\ \forall j,\ g,\ l,\ n$, and hence $\lim_{\epsilon'_f \to 0} \lambda = 0$, i.e., $\lim\limits_{\epsilon'_f \to 0} \rho = \lim\limits_{\epsilon_m \to 1} \rho = 0$ because $\rho = \max(|\lambda|)$. The proof is similar in TE where $\eta = \sqrt{\epsilon}$.

A.2. RCS (BA) = RCS (Isolated Disks) If (17) Is Satisfied

A.2.1. Derivation of RCS (BA)

In TM, the exact total field u is solution of $\Delta u + k_0^2(\epsilon_f + \epsilon_m)u = 0$ in V_s, with the incident plane wave u^{inc} as the source term. Let u_m be the solution of

$$\Delta u_m + k_0^2 \epsilon_m u_m = 0 \tag{A2}$$

in V_s with the same source term. Then

$$u = u_m + u_f \Longrightarrow \Delta u_f + k_0^2 \epsilon_m u_f = -k_0^2 \epsilon_f (u_m + u_f) \tag{A3}$$

the exact solution of which is

$$u_f(\underline{r}) = k_0^2 \int_{V_s} \epsilon_f\left(\underline{r}'\right) g_m\left(\underline{r}, \underline{r}'\right)\left[u_m\left(\underline{r}'\right) + u_f\left(\underline{r}'\right)\right] d\underline{r}' \tag{A4}$$

where g_m is the Green's function of the mean medium ϵ_m in V_s. When $\epsilon_m \simeq 1$, we let

$$u_m = u^{inc} + \delta u_m \tag{A5}$$

Then, because $\Delta u^{inc} + k_0^2 u^{inc} = 0$, (A2) yields $\Delta \delta u_m + k_0^2 \epsilon_m \delta u_m = k_0^2 u^{inc} \delta\epsilon_m$, hence:

$$\delta u_m(\underline{r}) = -k_0^2 \int_{V_s} \delta\epsilon_m\left(\underline{r}'\right) g_m\left(\underline{r}, \underline{r}'\right) u^{inc}\left(\underline{r}'\right) d\underline{r}' \tag{A6}$$

$g_m(\underline{r}, \underline{r}') = g_0(\underline{r}, \underline{r}') + \delta g_m(\underline{r}, \underline{r}')$ where $g_0(\underline{r}, \underline{r}') = -iH_0(k_0|\underline{r} - \underline{r}'|)/4$ is the free-space Green's function. Because δg_m and δu_m are of the first order in $\delta\epsilon_m$ and u_f is of the first order in ϵ_f, the first order term in (A4) [respectively (A6)] is $k_0^2 \int_{V_s} \epsilon_f(\underline{r}') g_0(\underline{r}, \underline{r}') u^{inc}(\underline{r}') d\underline{r}'$ [respectively $-k_0^2 \int_{V_s} \delta\epsilon_m(\underline{r}') g_0(\underline{r}, \underline{r}') u^{inc}(\underline{r}') d\underline{r}'$]. Then (A3) and (A5) imply that the total scattered field $u^s = u - u^{inc} = u_m + u_f - u^{inc} = u_f + \delta u_m$ writes, up to the first order in $\delta\epsilon_m$ and ϵ_f:

$$u^s(\underline{r}) = \frac{ik_0^2}{4} \int_{V_s} \left[\delta\epsilon_m\left(\underline{r}'\right) - \epsilon_f\left(\underline{r}'\right)\right] H_0\left(k_0\left|\underline{r} - \underline{r}'\right|\right) u^{inc}\left(\underline{r}'\right) d\underline{r}'$$

Because $u^{inc}(\underline{r}) = e^{-ik_0 r \underline{\widehat{k}} \cdot \underline{\widehat{r}}}$, we get (18) on account of (12). We proceed similarly in TE.

A.2.2. RCS (BA) = RCS (Isolated Disks)

The first term $\underline{c} = \mathbf{M}^{-1}\underline{a}$ in (15) yields, for Jacobi ($\mathbf{M} = \mathrm{diag}(\mathbf{S})$) and from (8), $c_j^n = a_j^n/d_j^n = i^n e^{ik_0 r_j \cos(\varphi_j - \varphi_0)} e^{-in\varphi_0}/d_j^n$; then the scattered corresponding far-field writes [see (13)]

$$F(\varphi) = \sum_{j=1}^{N_s} e^{ik_0\left(\widehat{\underline{r}}-\widehat{\underline{k}}\right)\cdot\underline{r}_j} \sum_{n=-\infty}^{\infty} (-1)^n e^{in(\varphi-\varphi_0)}/d_j^n$$

with $\underline{r}_j = (r_j, \varphi_j)$. In TM, when $x = k_0 a_j \to 0$, (A1) yields $1/d_j^0 = -i\pi k_0^2 \epsilon'_{fj} a_j^2/4$ with $\epsilon'_{fj} = \epsilon_{fj} + \delta\epsilon_{mj}$, and $1/d_j^n = 1/d_j^{-n} = o[(k_0 a_j)^2]$ $\forall n > 0$, hence:

$$F(\varphi) \sim -\frac{i\pi k_0^2}{4} \sum_{j=1}^{N_s} e^{ik_0\left(\widehat{\underline{r}}-\widehat{\underline{k}}\right)\cdot\underline{r}_j} \epsilon'_{fj} a_j^2 \tag{A7}$$

In TM, the scattered far-field (18) writes, if we let $\underline{r}' = \underline{r}_j + \underline{r}''$,

$$F_{\mathrm{BA}}(\varphi) \simeq -i\frac{k_0^2}{4} \sum_{j=1}^{N_s} \epsilon'_{fj} e^{ik_0\left(\widehat{\underline{r}}-\widehat{\underline{k}}\right)\cdot\underline{r}_j} \int_{V_j} e^{ik_0\left(\widehat{\underline{r}}-\widehat{\underline{k}}\right)\cdot\underline{r}''} d\underline{r}''$$

V_j is approximated by the disk of radius a_j. Then $\int_{V_j} e^{ik_0(\widehat{\underline{r}}-\widehat{\underline{k}})\cdot\underline{r}''} d\underline{r}'' = \int_0^{a_j} r'' dr'' \int_0^{2\pi} d\theta e^{ik_0|\widehat{\underline{r}}-\widehat{\underline{k}}|r''\cos\theta} = 2\pi \int_0^{a_j} r'' J_0(k_0|\widehat{\underline{r}} - \widehat{\underline{k}}|r'') dr'' \simeq \pi a_j^2$ because $k_0|\widehat{\underline{r}} - \widehat{\underline{k}}|r'' \leq 2k_0 a_j \ll 1$. This entails $\lim\limits_{k_0 a_j \to 0} F(\varphi) = F_{\mathrm{BA}}(\varphi)$ and RCS (BA) = RCS (isolated disks) if (17) is satisfied.

A.3. Derivation of the l.s.d. $\Sigma_{\mathbf{BA}}$ of the RCS

We assume that V_s is large. From (31), $s_{\mathrm{BA}} = s_f + s_m - 2s'_{mf}$ with $s'_{mf} = Re(s_{mf})$. Because $\langle s'_{mf}\rangle = 0$, $\langle s_{\mathrm{BA}}^2\rangle = s_m^2 + 2s_m\langle s_f\rangle + \langle s_f^2\rangle + 4\langle s'^2_{mf}\rangle - 4\langle s_f s'_{mf}\rangle$. (34) yields $\langle s_{\mathrm{BA}}\rangle^2 = \langle s_f\rangle^2 + s_m^2 + 2\langle s_f\rangle s_m$, hence:

$$\begin{aligned} \Sigma_B^2 &= \left\langle s_{\mathrm{BA}}^2 \right\rangle - \langle s_{\mathrm{BA}}\rangle^2 = \Sigma_f^2 + 4\left\langle s'^2_{mf}\right\rangle - 4\left\langle s_f s'_{mf}\right\rangle \\ \Sigma_f^2 &= \left\langle s_f^2 \right\rangle - \langle s_f\rangle^2 \end{aligned} \tag{A8}$$

Σ_f, $\langle s_f s'_{mf}\rangle$ and $\langle s'^2_{mf}\rangle$ are successively evaluated below.

A.3.1. Evaluation of Σ_f

From the definition (23) of the FT, $s_f(\varphi)$ defined by (31) writes, when $L \to \infty$, $s_f = k_0^3 \chi(\varphi)|\hat{\epsilon}_f(\underline{v}/2\pi)|^2/4$ or else, on account of (24), $s_f = A|\hat{\epsilon}_g(\underline{v}/2\pi)|^2$ where $A = \frac{k_0^3 \chi(\varphi) N_s}{4\sigma^2 V_s} \Phi_f(v/2\pi)$. Hence:

$$\left\langle s_f^2 \right\rangle = A^2 \left\langle |\hat{\epsilon}_g(\underline{v}/2\pi)|^4 \right\rangle \simeq A^2 \left(\frac{V_s}{N_s} \right)^4 \sum_{i,j,k,l=1}^{N_s} \langle \epsilon_{gi} \epsilon_{gj} \epsilon_{gk} \epsilon_{gl} \rangle$$
$$\times\, e^{-i\underline{v}\cdot(\underline{r}_i + \underline{r}_j - \underline{r}_k - \underline{r}_l)} \simeq A^2 \left(\frac{V_s}{N_s} \right)^4 \left[N_s \left\langle \epsilon_g^4 \right\rangle + 3N_s(N_s - 1)\sigma^4 \right]$$

On the other hand, $\langle s_f \rangle^2 = A^2 \langle |\hat{\epsilon}_g(\underline{v}/2\pi)|^2 \rangle^2 \simeq A^2 \sigma^4 V_s^4 / N_s^2$ from (22). This entails $\langle s_f^2 \rangle \simeq 3\langle s_f \rangle^2$ when $N_s \to \infty$ and $\Sigma_f \simeq \sqrt{2}\langle s_f \rangle$.

A.3.2. Evaluation of $\langle s_f s'_{mf} \rangle$

(31) implies $2s_f s'_{mf} = \frac{k_0^6}{16} \chi^2(\varphi) |F_f(\underline{v})|^2 [F_f(\underline{v}) F_m^*(\underline{v}) + F_f^*(\underline{v}) F_m(\underline{v})]$. $L \to \infty \Rightarrow F_f(\underline{v}) = \hat{\epsilon}_f^*(\underline{v}/2\pi)$ and (24) yields $|F_f(\underline{v})|^2 F_f(\underline{v}) \propto |\hat{\epsilon}_g(\underline{v}/2\pi)|^2 \hat{\epsilon}_g^*(\underline{v}/2\pi)$. As previously, the mean value of this discretized term is $\langle |\hat{\epsilon}_g(\underline{v}/2\pi)|^2 \hat{\epsilon}_g^*(\underline{v}/2\pi) \rangle \propto \sum_{i,j,k=1}^{N_s} \langle \epsilon_{gi} \epsilon_{gj} \epsilon_{gk} \rangle e^{i\underline{v}.(\underline{r}_i - \underline{r}_j - \underline{r}_k)} = 0$ because the r.v. ϵ_g is a centered white gaussian noise (in particular $\langle \epsilon_g^3 \rangle = 0$). Hence $\langle s_f s'_{mf} \rangle = 0$.

A.3.3. Evaluation of $\langle s'^2_{mf} \rangle$ and Derivation of (37)

$2s'_{mf} = \frac{k_0^3}{4} \chi(\varphi) [F_f(\underline{v}) F_m^*(\underline{v}) + F_f^*(\underline{v}) F_m(\underline{v})] \Rightarrow 4\langle s'^2_{mf} \rangle = \frac{k_0^6}{16} \chi^2(\varphi) [\langle F_f^2(\underline{v}) \rangle F_m^{*2}(\underline{v}) + 2\langle |F_f(\underline{v})|^2 \rangle |F_m(\underline{v})|^2 + \langle F_f^{*2}(\underline{v}) \rangle F_m^2(\underline{v})]$. It can easily be shown that $\langle F_f^2(\underline{v}) \rangle = \int_{V_s \times V_s} \langle \epsilon_f(\underline{r}') \epsilon_f(\underline{r}'') \rangle e^{i\underline{v}.(\underline{r}' + \underline{r}'')} d\underline{r}' d\underline{r}'' \simeq \Phi_f(v/2\pi) \int_{V_s} e^{2i\underline{v}.\underline{r}'} d\underline{r}'$. We finally get, because of (35),

$$4 \left\langle s'^2_{mf} \right\rangle \simeq \frac{k_0^6}{8} \chi^2(\varphi) \Phi_f(v/2\pi) \left\{ V_s |F_m(\underline{v})|^2 + \mathrm{Re}\left[F_m^2(\underline{v}) J_V(\underline{v}) \right] \right\}$$

with

$$J_V(\underline{v}) = \int_{V_s} e^{-2i\underline{v}\cdot\underline{r}'} d\underline{r}' \tag{A9}$$

and (A8) entails (37).

REFERENCES

1. Ishimaru, A., *Wave Propagation and Scattering in Random Media*, New York Academic Press, 1974.
2. Finson, M. L., "Hypersonic wakes aerodynamics at high reynolds numbers," *AIAA Journal*, Vol. 11, No. 8, 1137–1145 1973.
3. Levensteins, Z. J. and M. V. Krumins, "Aerodynamic characteristics of hypersonic wakes," *AIAA Journal*, Vol. 5, No. 9, 1596–1602, 1967.
4. Slattery, R. E. and W. G. Clay, "The turbulent wakes of hypersonic bodies," *17th Annual Meeting of the American Rocket Society*, 1962.
5. Stupfel, B., "A hybrid finite element and integral equation domain decomposition method for the solution of the 3-D scattering problem," *J. Comp. Phys.*, Vol. 172, 451–471, 2001.
6. Vouvakis, M. N., K. Zhao, S. M. Seo, and J. F. Lee, "A domain decomposition approach for non-conformal couplings between finite and boundary elements for unbounded electromagnetic problems in R3," *J. Comp. Phys.*, Vol. 225, 975–994, 2007.
7. Li, Y. J. and J. M. Jin, "Parallel implementation of the FETI-DPEM algorithm for general 3D electromagnetic simulations," *J. Comp. Phys.*, Vol. 228, 3255–3267, 2009.
8. Peng, Z. and J. F. Lee, "Non-conformal domain decomposition method with second order transmission conditions for time-harmonic electromagnetics," *J. Comp. Phys.*, Vol. 229, 5615–5629, 2010.
9. Bérenger, J. P., "Numerical reflection from FDTD-PMLs: A comparison of the split PML with the unsplit and CFS PMLs," *IEEE Trans. on Antennas and Propagat.*, Vol. 50, No. 3, 258–265, 2002.
10. Chen, Q., M. Katsurai, and P. Aoyagi, "An FDTD formulation for dispersive media using a current density," *IEEE Trans. on Antennas and Propagat.*, Vol. 46, No. 10, 1739–1745 1998.
11. Kong, J. A., *Electromagnetic Wave Theory*, John Wiley and Sons., 1986.
12. Jean, M., *Diffraction D'une Onde Électromagnétique Par Un Plasma Turbulent: Application Au Calcul De La Surface Equivalente Radar*, Thèse de l'Université Bordeaux I, 1995.
13. Tsang, L., C. E. Mandt, and K. H. Ding, "Monte Carlo simulations of the extinction rate of dense media with randomly distributed dielectric spheres based on solutions of Maxwell

equations," *Optics Lett.*, Vol. 17, No. 5, 314–316, 1992.
14. Elsherbeni, A. Z., M. Hamid, and G. Tian, "Iterative scattering of a gaussian beam by an array of circular conducting and dielectric cylinders," *Journal of Electromagnetic Waves and Applications*, Vol. 7, No. 10, 1323–1342, 1993.
15. Elsherbeni, A. Z. and A. A. Kishk, "Modeling of cylindrical objects by circular dielectric and conducting cylinders," *IEEE Trans. on Antennas and Propagat.*, Vol. 40, No. 1, 96–99, 1992.
16. Lin, J. H. and W. C. Chew, "BiCG-FFT T-matrix method for solving for the scattering solution from inhomogeneous bodies," *IEEE Trans. on Antennas and Propagat.*, Vol. 44, No. 7, 1150–1155, 1996.
17. Le Ravalec, M., B. Noetinger, and L. Y. Hu, "The FFT moving average (FFT-MA) generator: An efficient numerical method for generating and conditionning Gaussian simulations," *Mathematical Geology*, Vol. 32, No. 6, 701–723, 2000.
18. Bardon, M., *Etude théorique Et Expérimentale De La Polarisation Du Rayonnement Diffusé Par Une Surface Rugueuse. Application À La Détection De Rayures*, Thèse de l'Ecole Centrale Paris, 2003.
19. Gradshteyn, I. S. and I. M. Ryzhik, *Table of Integrals, Series and Products*, Academic Press, 1980.
20. Abramowitz, M. and I. E. Stegun, *Handbook of Mathematical Functions*, 1972.
21. Bonnemason, P., R. Le Martret, and B. Stupfel, "Oblique incidence scattering by large, coated cylinders of arbitrary cross-section," *URSI Digest of the Joint Symposia IEEE-APS/URSI/NEM*, Vol. 26, Chicago, July 1992.
22. Chew, W. C., "Recurrence relations for 3D scalar addition theorem," *Journal of Electromagnetic Waves and Applications*, Vol. 6, Nos. 1–4, 133–142, 1992.
23. Chew, W. C. and Y. M. Wang, "Efficient way to compute the vector addition theorem," *Journal of Electromagnetic Waves and Applications*, Vol. 7, No. 5, 651–665 1993.